UC Irvine
UC Irvine Previously Published Works

Title
Visualizing association of N-ras in lipid microdomains: influence of domain structure and interfacial adsorption.

Permalink
https://escholarship.org/uc/item/9f54k8kz

Journal
Journal of the American Chemical Society, 128(1)

ISSN
0002-7863

Authors
Nicolini, Chiara
Baranski, Jörg
Schlummer, Stefanie
et al.

Publication Date
2006

DOI
10.1021/ja055779x

Copyright Information
This work is made available under the terms of a Creative Commons Attribution License, availalbe at https://creativecommons.org/licenses/by/4.0/

Peer reviewed

eScholarship.org Powered by the California Digital Library
University of California

J|A|C|S
ARTICLES
Published on Web 12/09/2005

Visualizing Association of N-Ras in Lipid Microdomains: Influence of Domain Structure and Interfacial Adsorption

Chiara Nicolini,[†] Jörg Baranski,[†] Stefanie Schlummer,[‡] José Palomo,[‡] Maria Lumbierres-Burgues,[‡] Martin Kahms,[§] Jürgen Kuhlmann,[§] Susana Sanchez,[||] Enrico Gratton,[||] Herbert Waldmann,[‡] and Roland Winter*[,†]

Contribution from Physical Chemistry I—Biophysical Chemistry and Organic Chemistry, Department of Chemistry, University of Dortmund, Otto-Hahn-Strasse 6, D-44227 Dortmund, Germany, Departments of Chemical and Structural Biology, Max Planck Institute of Molecular Physiology, Otto-Hahn-Strasse 11, D-44227 Dortmund, Germany, and Laboratory for Fluorescence Dynamics, University of Illinois, Urbana, Illinois 61801

Received August 23, 2005; E-mail: winter@pci.chemie.uni-dortmund.de

Abstract: In this study, two-photon fluorescence microscopy on giant unilamellar vesicles and tapping-mode atomic force microscopy (AFM) are applied to follow the insertion of a fluorescently (4,4-difluoro-4-bora-3a,4a-diaza-*s*-indacene, BODIPY) labeled and completely lipidated (hexadecylated and farnesylated) N-Ras protein into heterogeneous lipid bilayer systems. The bilayers consist of the canonical raft mixture 1-palmitoyl-2-oleoylphosphatidylcholine (POPC), sphingomyelin, and cholesterol, which—depending on the concentration of the constituents—separates into liquid-disordered (l_d), liquid-ordered (l_o), and solid-ordered (s_o) phases. The results provide direct evidence that partitioning of N-Ras occurs preferentially into liquid-disordered lipid domains, which is also reflected in a faster kinetics of incorporation into the fluid lipid bilayers. The phase sequence of preferential binding of N-Ras to mixed-domain lipid vesicles is $l_d > l_o \gg s_o$. Intriguingly, we detect, using the better spatial resolution of AFM, also a large proportion of the lipidated protein located at the l_d/l_o phase boundary, thus leading to a favorable decrease in line tension that is associated with the rim of the demixed phases. Such an interfacial adsorption effect may serve as an alternative vehicle for association processes of signaling proteins in membranes.

Introduction

Ras proteins belong to the Ras superfamily of low-molecular-weight GTPases that serve as GDP/GTP-regulated relay switches. Ras function is known to be crucially dependent on its association with the inner leaflet of the plasma membrane. Three isoforms of Ras, H-Ras and N-Ras, which traffic through the Golgi to the plasma membrane, and K-Ras, which traffics via a cytosolic pathway, are expressed in mammalian cells.[1,2] They generate distinct signal outputs, despite interacting with a common set of activators and effectors. The Ras signaling pathway is central to the regulation of cell growth and differentiation, and impaired Ras function can be one of the critical steps leading to cell transformation. The importance of the correct functioning of the Ras cascade is illustrated by the fact that point mutations in the Ras oncogenes, usually in N- or K-Ras, are found in approximately 30% of all human cancers.[3]

To perform their normal and oncogenic functions, Ras proteins must be membrane-associated. Their membrane targeting and membrane binding is controlled by posttranslational covalent attachment of lipid groups. Lipidation is believed to play an important role in regulatory functions, for example, by mediating protein—protein and protein—lipid interactions. The association with different membrane microenvironments is proposed to further regulate Ras signaling mechanisms. In this context, it has also become clear that the differential lateral segregation of Ras isoforms, namely, N-, H- and K-Ras, would offer a plausible mechanism for the distinct signal outputs of these highly homogeneous proteins.[2] The membrane anchors of H-, N-, and K-Ras comprise a common C-terminal S-farnesylcysteine carboxymethyl ester, operating in concert with one or two adjacent *S*-palmitoylcysteine residues in N- and H-Ras, and with a polybasic domain of six lysines in K-Ras.

Specific lipid modifications of proteins are believed to be sufficient to sequester them in certain microdomains, such as lipid rafts and caveolae. Measurements of green fluorescent proteins with different types of lipid anchors indicated that the myristoyl and palmitoyl groups promote clustering in rafts whereas isoprenyl groups do not.[4] Additionally, not only the structure of lipid modifications but also the position of their

[†] Physical Chemistry I—Biophysical Chemistry, Department of Chemistry, University of Dortmund.
[‡] Department of Chemical Biology, Max Planck Institute of Molecular Physiology, and Organic Chemistry, Department of Chemistry, University of Dortmund.
[§] Department of Structural Biology, Max Planck Institute of Molecular Physiology.
[||] University of Illinois.

(1) Wittinghofer, A.; Waldmann, H. *Angew. Chem., Int. Ed.* **2000**, *39*, 4192—4214.
(2) Hancock, J. F. *Nat. Rev. Mol. Cell Biol.* **2003**, *4*, 373—383.
(3) Bos, J. L. *Cancer Res.* **1989**, *49*, 4682—4689.
(4) Zacharias, D. A.; Violin, J. D.; Newton, A. C.; Tsien, R. Y. *Science* **2002**, *296*, 913—916.

10.1021/ja055779x CCC: $33.50 **© 2006 American Chemical Society**

attachment seems to influence the affinity for specific membrane domains, at least in small model peptides.[5] Therefore, the question arises how the lipidation pattern of palmitoylated and farnesylated Ras proteins affects their localization to different membrane microdomains. Furthermore, the importance of domain boundary effects for partitioning of the lipidated protein has to be explored. The importance of such effects has been raised by computer simulation studies.[6−8]

The multicomponent character of biomembranes leads to strong membrane heterogeneity and phase segregation originating from compositional fluctuations. In the state of equilibrium, lipid phase separation leads to the formation of macroscopically large domains (phases), whereas out of equilibrium, the phase separation process may produce small-scale domains and extended compositional fluctuations may be observed. An interesting issue is related to the existence of lipid domains on the nanometer (1−100 nm) to micrometer (1−30 μm) scale and the relationship between lipid-domain formation and the conformation and functional properties of membrane-associated proteins.[9−17] There has been considerable interest in the possibility that the plasma membrane contains lipid "rafts", microdomains enriched in cholesterol and sphingolipids, and it has been suggested that such rafts could play an important role in many cellular processes including signal transduction, cell adhesion, apoptosis, and sorting and transport of lipids and proteins (for a critical account, see, for example, the review by Munro[13]). The domain organization and the connectivity properties of different domain regions will certainly have consequences for the diffusional properties of membrane-bound molecules, such as receptors, and may hence control the kinetics and reaction yields of the associated biochemical reactions. Possible scenarios include accumulation and colocalization of receptors and ligands in the same membrane compartments via cooperative domain-organization processes. To what extent domains actually exist in vivo remains still controversial, however.[13,14]

To understand the role of lipid complexes and (probably transient) clusters or domains in regulating membrane properties, ternary mixtures containing cholesterol and a saturated and an unsaturated phospholipid are often chosen in model studies of rafts. Along with a number of techniques used to address questions on rafts, important contributions have come from different microscopic approaches such as two-photon excited fluorescence microscopy[18−27] and, more recently, atomic force microscopy (AFM)[28−35] for studying solid-supported membranes. The fluorescence microscopy experiments—with a spatial resolution on the micrometer scale—on giant unilamellar vesicles (GUVs) prepared from particular three-component lipid raft mixtures indicate the coexistence of two fluid phases [liquid-disordered (l_d) and liquid-ordered (l_o)]. However, in natural cell membranes, there are a variety of factors (e.g., membrane proteins) that limit the size of rafts to considerably smaller dimensions than those reported in model membranes by use of fluorescence microscopy. Various biophysical techniques were used to measure the size of lipid rafts in vivo, yielding values as low as about 5 nm.[36] In a recent work we have demonstrated the existence of small- and intermediate-scale compositional fluctuations and domains of "canonical" raft mixtures, using small-angle neutron scattering (SANS) with H/D contrast variation.[37,38] The data clearly indicate the existence of microdomains in the model raft mixtures, not only in the micrometer range as revealed by fluorescence microscopy but also over a large length scale down to the biologically more relevant range of several tens of nanometers. Lipid−lipid interactions obviously can originate lipid rafts on very different length scales. Domains in the range of several tens of nanometers have been detected by AFM studies on canonical raft mixtures as well,[28−35] an approach for high-resolution imaging of membrane heterogeneity on a length scale of tens of nanometers. Hence, by combining both methods, we are able to cover the full range of domain sizes from micrometers to nanometers.

Recently, we studied the effects of a fluorescent peptide containing a farnesyl (Far) and palmitoyl (Pal) anchor, BODIPY-Gly-Cys(Pal)-Met-Gly-Leu-Pro-Cys(Far)-OMe, which represents a membrane recognition model system for Ras proteins, on model membranes consisting of the binary phospholipid mixture DMPC (dimyristoylphosphatidylcholine)/DSPC (distearoylphosphatidylcholine) and varying levels of cholesterol.[39] Here, we present for the first time data on the partitioning of a fluorescently (4,4-difluoro-4-bora-3a,4a-diaza-*s*-indacene, BODIPY) labeled and completely lipidated N-Ras protein in giant unilamellar vesicles of model raft mixtures. To observe the

(5) Wang, T.-Y.; Leventis, R.; Silvius, J. R. *Biochemistry* **2001**, *40*, 13031−13040.
(6) Dumas, F.; Sperotto, M. M.; Lebrun, M. C.; Tocanne, J. F.; Mouritsen, O. G. *Biophys. J.* **1997**, *73*, 1940−1953.
(7) Nielsen, L. K.; Vishnyakov, A.; Jørgensen, K.; Bjørnholm, T.; Mouritsen, O. G. *J. Phys.: Condens. Matter* **2000**, *12*, A309-A314.
(8) Mouritsen, O. G. *Life−As a matter of fat*; Springer-Verlag: Berlin, 2005.
(9) Simons, K.; Ikonen, E. *Nature* **1997**, *387*, 569−572.
(10) Silvius, J. R. *Biochim. Biophys. Acta* **2003**, *1610*, 174−183.
(11) Anderson, R. G. W.; Jacobson, K. *Science* **2002**, *296*, 1821−1825.
(12) Edidin, M. *Annu. Rev. Biophys. Biomol. Struct.* **2003**, *32*, 257−283.
(13) Munro, S. *Cell* **2003**, *115*, 377−388.
(14) Mukherjee, S.; Maxfield, F. R. *Annu. Rev. Cell. Dev. Biol.* **2004**, *20*, 839−866.
(15) London, E.; Brown, D. A. *Biochim. Biophys. Acta* **2000**, *1508*, 182−195.
(16) Lai, E. C. *J. Cell Biol.* **2003**, *162*, 365−370.
(17) Simons, K.; Vaz, W. L. C. *Annu. Rev. Biophys. Biomol. Struct.* **2004**, *33*, 269−295.
(18) Bagatolli, L. A.; Gratton, E. *Biophys. J.* **2000**, *79*, 434−447.
(19) Baumgart, T.; Hess, S. T.; Webb, W. W. *Nature* **2003**, *425*, 821−824.
(20) Bagatolli, L. A. *Chem. Phys. Lipids* **2003**, *122*, 137−145.
(21) Korlach, J.; Schwille, P.; Webb, W. W.; Feigenson, G. W. *Proc. Natl. Acad. Sci. U.S.A.* **1999**, *96*, 8461−8466.
(22) De Almeida, R. F. M.; Federov, A.; Prieto, M. *Biophys. J.* **2003**, *85*, 2406−2416.
(23) Dietrich, C.; Bagatolli, L. A.; Volovyk, Z. N.; Thompson, N. L.; Levi, M.; Jacobson, K.; Gratton, E. *Biophys. J.* **2001**, *80*, 1417−1428.
(24) Veatch, S. L.; Keller, S. L. *Phys. Rev. Lett.* **2002**, 268101.
(25) Veatch, S. L.; Polozov, I. V.; Gawrisch, K.; Keller, S. L. *Biophys. J.* **2004**, *86*, 2910−2922.
(26) De Almeida, R. F. M.; Loura, L. M. S.; Fedorov, A.; Prieto, M. *J. Mol. Biol.* **2004**, *346*, 1109−1120.
(27) Fahsel, S.; Pospiech, E.-M.; Zein, M.; Hazlett, T. L.; Gratton, E.; Winter, R. *Biophys. J.* **2002**, *83*, 334−344.
(28) Rinia, H. A.; Snel, M. M. E.; Van der Eerden, J. P. J. M.; de Kruijff, B. *FEBS Lett.* **2002**, *501*, 92−96.
(30) Milhiet, P. E.; Domec, C.; Giocondi, M.-C.; van Mau, N.; Heitz, F.; le Grimellec, C. *Biophys. J.* **2001**, *81*, 547−555.
(31) Jass, J.; Tjärnhage, T.; Puu, G. *Biophys. J.* **2000**, *79*, 3153−3163.
(32) Richter, R.; Mukhopadhyay, A.; Brisson, A. *Biophys. J.* **2003**, *85*, 3035−3047.
(33) Lawrence, J. C.; Saslowsky, D. E.; Edwardson, J. M.; Henderson, R. M. *Biophys. J.* **2003**, *84*, 1827−1832.
(34) Saslowsky, D. E.; Lawrence, J.; Ren, X.; Brown, D. A.; Henderson, R. M.; Edwardson, J. M. *J. Biol. Chem.* **2002**, *277*, 26966−26970.
(35) Milhiet, P.-E.; Giocondi, M.-C.; Baghdadi, O.; Ronzon, F.; Roux, B.; Le Grimellec, C. *EMBO Rep.* **2002**, *3*, 485−490.
(36) Tokumasu, F.; Jin, A. J.; Feigenson, G. W.; Dvorak, J. A. *Biophys. J.* **2003**, *84*, 2609−2618.
(37) Lommerse, P. H. M.; Blab, G. A.; Cognet, L.; Harms, G. S.; Snaar-Jagalska, B. E. *Biophys. J.* **2001**, *86*, 609−616.
(38) Winter, R.; Gabke, A.; Czeslik, C.; Pfeifer, P. *Phys. Rev. E* **1999**, *60*, 7354−7359.
(39) Nicolini, C.; Winter, R.; Thiyagarajan, P. *Phys. Chem. Chem. Phys.* **2004**, *6*, 5531−5534.
(40) Janosch, S.; Nicolini, C.; Ludolph, B.; Peters, C.; Völkert, M.; Hazlet, T. L.; Gratton, E.; Waldmann, H.; Winter, R. *J. Am. Chem. Soc.* **2004**, *126*, 7496−7503.

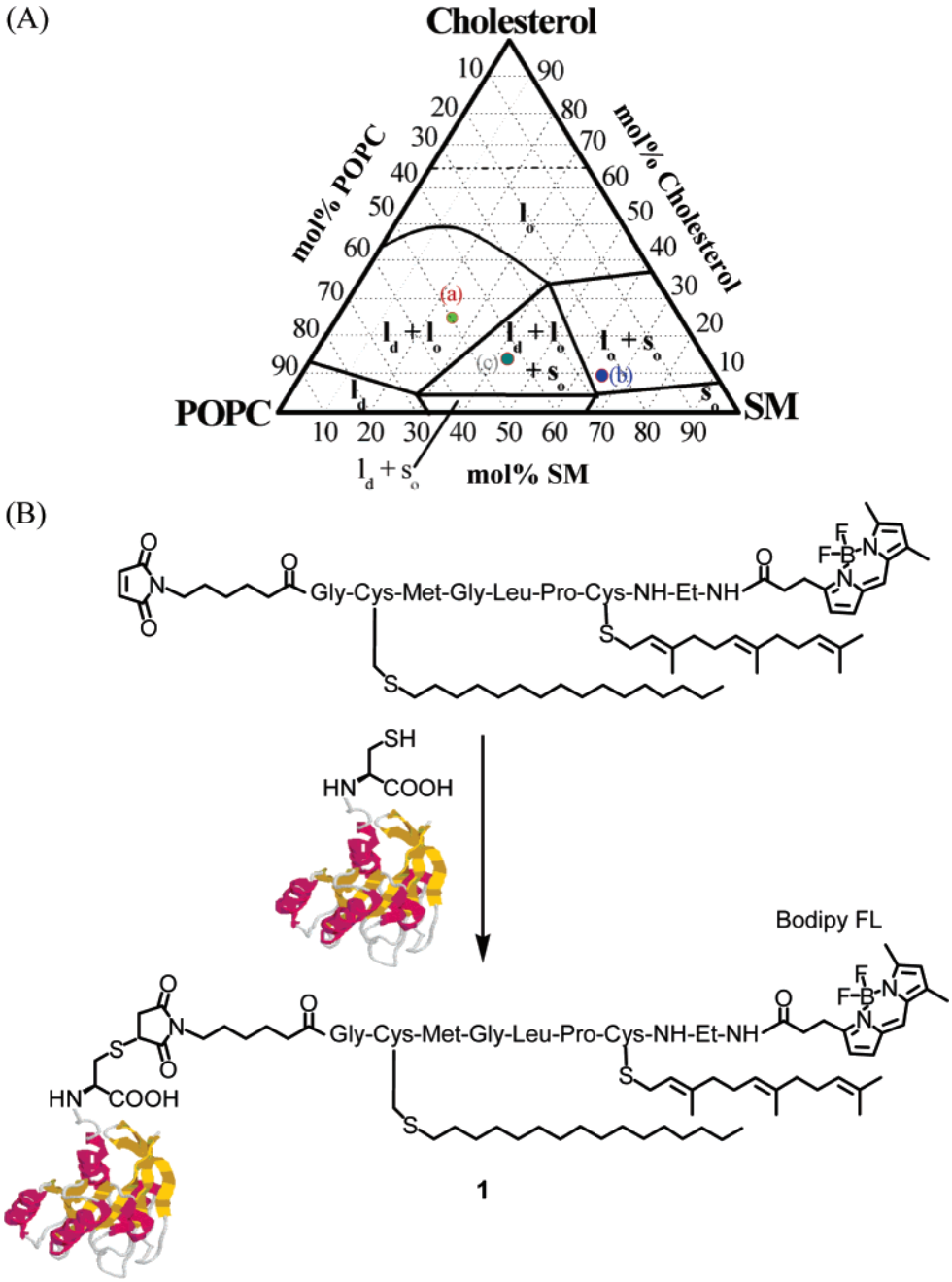

Figure 1. (A) POPC/BSM/cholesterol phase diagram at $T = 23$ °C (adapted from ref 22). Circles a−c denote lipid compositions where experimental data have been taken: (a) POPC/BSM/Chol (50:25:25), $l_d + l_o$ phase coexistence region; (b) POPC/BSM/Chol (25:65:10), $l_d + l_o + s_o$ phase coexistence region; (c) POPC/BSM/Chol (43:43:14), $l_o + s_o$ phase coexistence region. (B) Schematic synthesis of the semisynthetic N-Ras protein.

heterogeneous membrane structure, two-photon excitation fluorescence microscopy techniques are used, complemented by atomic force microscopy (AFM) measurements to additionally probe the partitioning on the nanometer length scale. We worked with three different lipid compositions of the system POPC/BSM/Chol to analyze the protein binding properties in various coexisting lipid phase regions. A phase diagram of the ternary system POPC/SM/Chol at room temperature is given in De Almeida et al. (Figure 1A).[22]

Materials and Methods

Sample Preparation: (a) Lipids. 1-Palmitoyl-2-oleoyl-*sn*-glycero-3-phosphocholine (POPC) and brain sphingomyelin (BSM) were purchased from Avanti Polar Lipids (Birmingham, AL), and cholesterol (Chol) was from Sigma−Aldrich (Deisenhofen). Stock solutions of the lipids POPC/BSM/cholesterol in 50:25:25, 43:43:14, and 25:65:10 (mol %) ratios were mixed in 0.2 mg/mL chloroform/methanol (4:1). The fluorescent probe *N*-Rh-DPPE (Lissamine rhodamine B, 1,2-dihexadecanoyl-*sn*-glycero-3-phosphoethanolamine) was obtained from Molecular Probes (Eugene, OR).

(b) N-Ras. Fluorescently labeled N-Ras protein **1** was synthesized as described previously.[40] Briefly, the lipid-modified peptide derivatized at the N-terminus with a maleimidocaproic acid (MIC) amide and at the C-terminus with a 2-aminoethyl amide was synthesized on a chlorotrityl resin. The BODIPY-FL label was then introduced by acylation of the primary amine at the C-terminus. Finally, the maleimido peptide was coupled to a bacterially expressed truncated N-Ras protein

(41) Reents, R.; Wagner, M.; Schlummer, S.; Kuhlmann, J.; Waldmann, H. *ChemBioChem* **2005**, *6*, 86−94.

(amino residues 1−181) carrying a cysteine at the C-terminus. Coupling was achieved by conjugate addition of the only surface-accessible cysteine-SH group to the maleimido function.[41]

To ensure that the replacement of the natural carboxymethyl group at the C-terminal cysteine by the BODIPY-FL label did not influence the partitioning of the N-Ras lipoprotein in the lipid vesicles, we generated an additional labeled protein construct, with an identical MIC lipopeptide differing only in the fact that it did contain the original carboxymethyl function. Here, the fluorescent label was introduced into the protein corpus prior to MIC coupling. For this purpose 12 mg of truncated N-Ras (N-Ras1−181) was incubated with a 5-fold molar excess of NHS-BODIPY in 0.1 M Na_2CO_3/$NaHCO_3$, pH 8.5, at 4 °C for 30 min, resulting in the reaction with surface-exposed lysine side chains at statistical positions. Free dye was separated from the labeled protein by intensive dialysis against 20 mM Tris and 5 mM $MgCl_2$, pH 7.4. The labeling efficiency was calculated by determining the ratio of BODIPY (absorption at 504 nm) to protein (Bradford assay) and was estimated to be around 20−30%. The different samples showed the same partitioning pattern (data not shown), as could be expected from the distant location of the fluorophore from the lipid anchor system.

Fluorescence Microscopy: (a) Vesicle Preparation. For preparing giant unilamellar vesicles (GUVs), we followed the electroformation method developed by Angelova and Dimitrov and co-workers.[42,43] GUVs provide a free-standing bilayer, without potential substrate effects. To grow the GUVs, a special temperature-controlled chamber was used, which was described previously.[44] The experiments were carried out in the same chamber after vesicle formation, by use of an inverted microscope (Axiovert 35; Zeiss, Thornwood, NY). The following steps were used to prepare the GUVs: (1) The lipid solution (2 μL) was spread on each platinum (Pt) wire under a stream of N_2. To remove residues of the organic solvent, the samples were lyophilized for 1 h. (2) To add the aqueous solvent into the chamber (Millipore water, 17.5 MΩ·cm), the bottom part of the chamber was sealed with a coverslip. Water previously heated at 61 °C (2 mL) was added to cover the Pt wires. After this step, the Pt wires were connected to a function generator (Hewlett-Packard, Santa Clara, CA), and a low-frequency AC field (sinusoidal wave function with a frequency of 10 Hz and an amplitude of 2 V) was applied for 90 min. After vesicle formation, the AC field was turned off and the temperature scan (from high to low temperatures) was initiated. A charge-coupled device color video camera (CCD-Iris; Sony, Tokyo) attached to the microscope was used to follow the vesicle formation and to select a target vesicle. The temperature was measured inside the sample chamber with a digital thermocouple (model 400B; Omega, Stamford, CT) with a precision of 0.1 °C. The fluorescent probe was premixed with the lipids in chloroform. The *N*-Rh-DPPE/lipid ratio used was 1:400 (mol/mol) in the two-channel experiment.

(b) Experimental Setup. The two-photon excitation microscopy experiments were performed at the Laboratory for Fluorescence Dynamics (University of Illinois at Urbana−Champaign). The high photon densities required for two-photon absorption are achieved by focusing a high peak power laser light source on a diffraction-limited spot through a high numerical aperture objective. Therefore, in the areas above and below the focal plane, two-photon absorption does not occur because of insufficient photon flux. This allows a sectioning effect without the use of emission pinholes as in confocal microscopy. Another advantage of two-photon excitation is the low extent of photobleaching and photodamage above and below the focal plane. For our experiments, we used a scanning two-photon fluorescence microscope[45,46] with an LDAchroplan 20× long working distance air objective (Zeiss, Homldale, NJ) with a numerical aperture of 0.4. A titanium−sapphire laser (Mira 900; Coherent, Palo Alto, CA), pumped by a frequency-doubled Nd:vanadate laser was used as excitation light source. The excitation wavelength was set at 780 nm. The laser was guided by a galvanometer-driven $x-y$ scanner (Cambridge Technology, Watertown, MA) to achieve beam scanning in both the x and y directions. The scanning rate was controlled by the input signal from a frequency synthesizer (Hewlett-Packard, Santa Clara, CA), and a frame rate of 25 s was used to acquire the images (256 × 256 pixels). The fluorescence emission was observed through a broad band-pass filter from 350 to 600 nm (BG39 filter; Chroma Technology, Brattleboro, VT). For detecting both fluorophore emissions simultaneously in two channels, a fluorescein/Texas red filter set was used to collect fluorescence in the green and red regions, respectively. The green emission filter was a Chroma HQ525/50 (500−550 nm), the red was a Chroma HQ610/75 (573−648 nm), and the dichroic was a Q560LP. Both of the emission filters were coated for multiphoton work. A miniature photomultiplier (R5600-P; Hamamatsu, Bridgewater, NJ) was used for light detection in the photon counting mode.

Atomic Force Microscopy: (a) Sample Preparation. For the AFM studies, the protein was lyophilized in 20 mM Tris buffer and 5 mM $MgCl_2$. Stock solutions of 2 mg/mL lipid (POPC, BSM, and cholesterol) in chloroform (Merck, Darmstadt) were prepared and mixed to obtain 2 mg of total lipid with the desired compositions. After the majority of the chloroform was evaporated with a nitrogen stream, all solvent was removed by drying under vacuum overnight. The dry lipid mixture was then hydrated with 1 mL of 20 mM NaCl, vortexed, and kept in a water bath at 70 °C for 1 h. After five freeze−thaw cycles, large multilamellar vesicles were formed and transformed to small unilamellar vesicles (SUV) by use of an extruder (Avanti Polar Lipids. Alabaster, AL) with polycarbonate filter of 0.1 μm pore size at 70 °C. Supported lipid bilayers for AFM measurements were produced by depositing 20 μL of the lipid vesicle solution with 50 μL of *N*-(2-hydroxyethyl)-piperazine-*N*′-2-ethanesulfonic acid (HEPES) buffer (pH 7.4) on freshly cleaved mica for 15 min. After the incubation time, the sample was rinsed carefully with HEPES buffer and placed on the AFM stage.

(b) AFM Setup. Measurements were conducted on a multimode scanning probe microscope (Digital Instruments, Santa Barbara, CA) with an E-scanner (15 μm). Images were obtained applying the tapping in liquid method with oxide-sharpened silicon nitride probes (NP-S, Veeco Instruments) mounted in a fluid cell (MTFML and MMTMEC, Veeco Instruments). Tips with nominal force constants from 0.06 to 0.32 N/m were used at driving frequencies ranging from 7 to 10 kHz corresponding to the softness of the sample. Height and phase images of sample regions between 0.5 and 5.0 μm were acquired with resolutions of 512 × 512 pixels and scan frequencies between 0.4 and 2.0 Hz. All measurements were carried out at room temperature (~25 °C).

Results and Discussion

Two-Photon Excited Fluorescence Microscopy. Confocal fluorescence microscopy has enabled the direct observation and analysis of phase domains in giant unilamellar vesicles (GUVs). Phases can be identified as ordered or fluidlike disordered on the basis of the known partition behavior of appropriate fluorescence probes. We studied GUVs formed from ternary mixtures of the lipids 1-palmitoyl-2-oleoylphosphatidylcholine (POPC), bovine sphingomyelin (BSM), and cholesterol (Chol). Sphingomyelin and cholesterol enrich in an ordered lipid phase with short-range order, whereas POPC prefers a disordered (l_d)

(42) Bader, B.; Kuhn, K.; Owen, D. J.; Waldmann, H.; Wittinghofer, A.; Kuhlmann, J. *Nature* **2000**, *403*, 223−226.
(43) Angelova, M. I.; Dimitrov, D. S. *Faraday Discuss. Chem. Soc.* **1986**, *81*, 303−311.
(44) Angelova, M. I.; Soléau, S.; Meléard, Ph.; Faucon, J. F.; Bothorel, P. *Prog. Colloid Polym. Sci.* **1992**, *98*, 127−131.
(45) Bagatolli, L. A.; Gratton, E. *Biophys. J.* **1999**, *77*, 2090−2101.
(46) So, P. T. C.; French, T.; Yu, W. M.; Berland, K. M.; Dong, C. Y.; Gratton, E. *Bioimaging* **1995**, *3*, 49−63.
(47) So, P. T. C.; French, T.; Yu, W. M.; Berland, K. M.; Dong, C. Y.; Gratton, E. In *Fluorescence Imaging Spectroscopy and Microscopy*; Wang, X. F., Herman, B., Eds.; Chemical Analysis Series, Vol. 137, John Wiley and Sons: New York, 1996; pp 353−374.

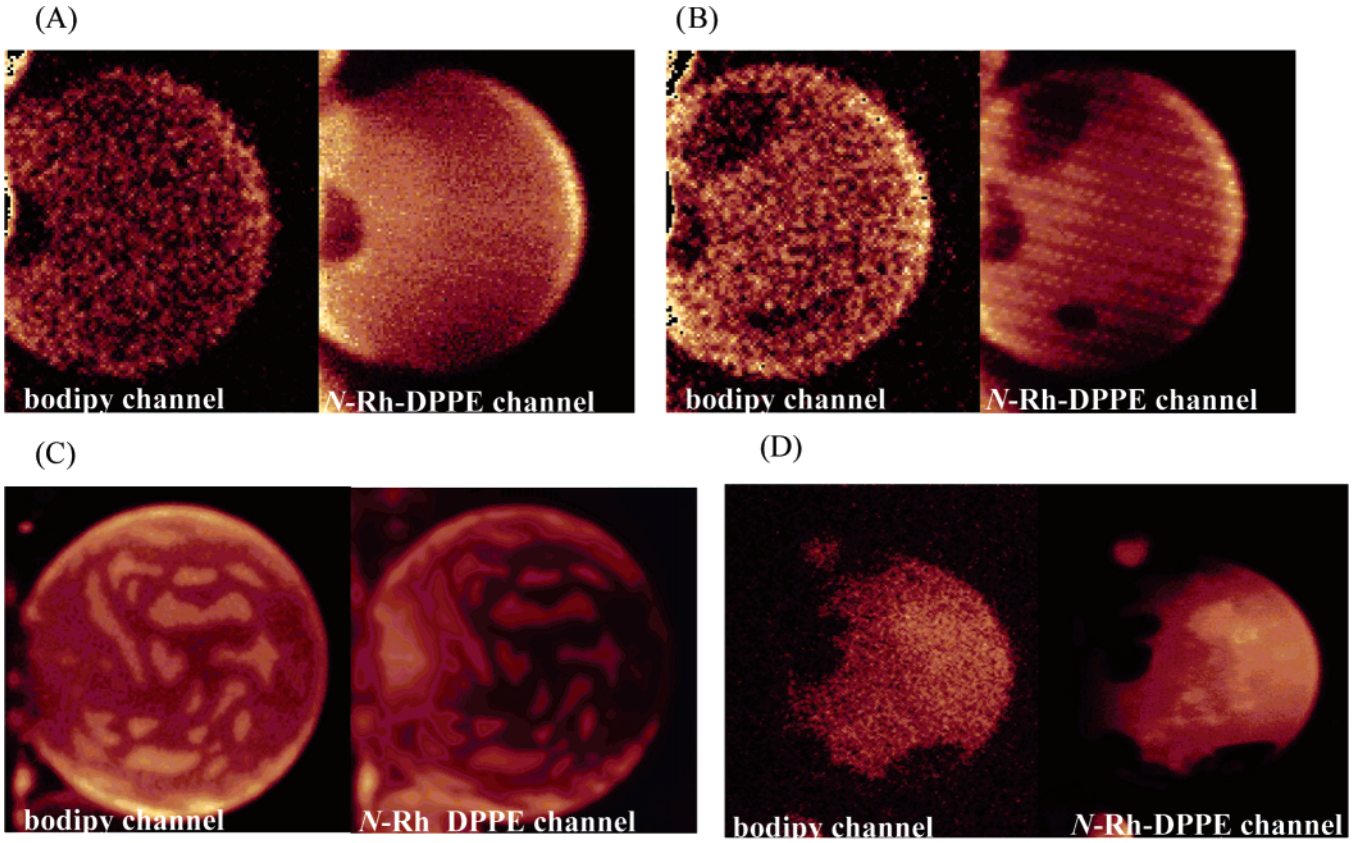

Figure 2. Two-photon excitation fluorescence intensity images (false color representation) of GUVs (size ~30 μm) consisting of (A, B) POPC/BSM/Chol (50:25:25) + 7 mol % N-Ras at $T = 25$ °C ($l_d + l_o$ phase), (C) POPC/BSM/Chol (25:65:10) + 7 mol % N-Ras at $T = 30$ °C ($l_o + s_o$ phase), and (D) POPC/BSM/Chol (43:43:14) + 7 mol % N-Ras at $T = 29$ °C ($l_d + l_o + s_o$ phase). Fluorescence intensity was collected in two channels: the green channel detects the BODIPY fluorescence intensity; and the red channel, the *N*-Rh-DPPE fluorescence intensity. Images were taken at the top part of the GUVs.

phase. The phase diagram of this lipid mixture at physiologically relevant temperatures shows a large binary coexistence region of liquid-disordered (l_d) and liquid-ordered (l_o) domains, such as for the composition POPC/BSM/Chol 50:25:25 (mol %) (Figure 1A).[22] By varying the lipid composition, further phase coexistence regions can be prepared, such as a $l_o + s_o$ phase coexistence region from POPC/BSM/Chol 25:65:10 and a $l_o + l_d + s_o$ three-phase region from POPC/BSM/Chol 43:43:14.

We prepared vesicles mixing the lipids with *N*-Rh-DPPE and added to the solution containing GUVs at ~30 °C a 7 mol % (with respect to lipid) solution of the hexadecylated and farnesylated N-Ras in 1 mM phosphate buffer (pH 7). The Ras lipoprotein was equipped with a hexadecyl thioether instead of the labile native palmitoyl thioester to prevent hydrolysis of the acyl function during the experiments. *N*-Rh-DPPE serves as a well-known marker of the POPC-rich liquid-disordered phase (red channel),[39] and the BODIPY label attached to the protein reports on the location of the protein within the lipid assembly (green channel). To reveal if *N*-Rh-DPPE partitions into a $l_o + s_o$ lipid mixture, we measured the partitioning of this dye with respect to that of Prodan, which is known to preferentially partition into the more disordered, l_o phase in such mixtures.[47,16] As expected, *N*-Rh-DPPE inserts into the same domains as Prodan does (data not shown), indicating that *N*-Rh-DPPE is also suitable for detecting l_o domains if no liquid-disordered phase is present.

The GUV images, taken after the protein binding process to the various lipid vesicle systems was completed, are shown in Figure 2. Panels A and B exhibit the round-shaped domains typical for coexisting liquidlike phases.[18,20,27] The bright areas with embedded *N*-Rh-DPPE correspond to liquid-disordered (l_d) domains; the dark domains mainly consist of l_o lipid. The domain shapes seen in panels C and D have different patterns, pointing to the presence of some solid-ordered gel phases. Please note that differences in the qualities of images A, B and C are due to experimental factors, such as the momentary laser power, the number of integrations used for collecting the data, and the state of the dye, that is, the degree of photobleaching. We are able to follow directly how the protein binds to the lipid microdomains through the simultaneous comparison of the images shown in the rhodamine and BODIPY channels. As we can clearly see from the GUV images of both channels, the spatial distribution of the inserted N-Ras coincides with that of the *N*-Rh-DPPE in all cases. Both are preferentially localized in the l_d domains of the mixed $l_d + l_o$ system (Figure 2A,B). The same holds true for the $l_d + l_o + s_o$ phase coexistence region (Figure 2D). In the mixed-domain $l_o + s_o$ region, however, preferential partitioning occurs in the l_o phase (Figure 2C).

The fluorescence technique can also be applied to yield kinetic data on the insertion process of the protein into GUVs. An example is given in Figure 3. We show fluorescence microscopy images of the GUVs in the two channels taken after the injection of N-Ras solution into the dispersion of lipid vesicles being in

(48) Bagatolli, L. A.; Gratton, E. *J. Fluoresc.* **2001**, *11*, 141−160.

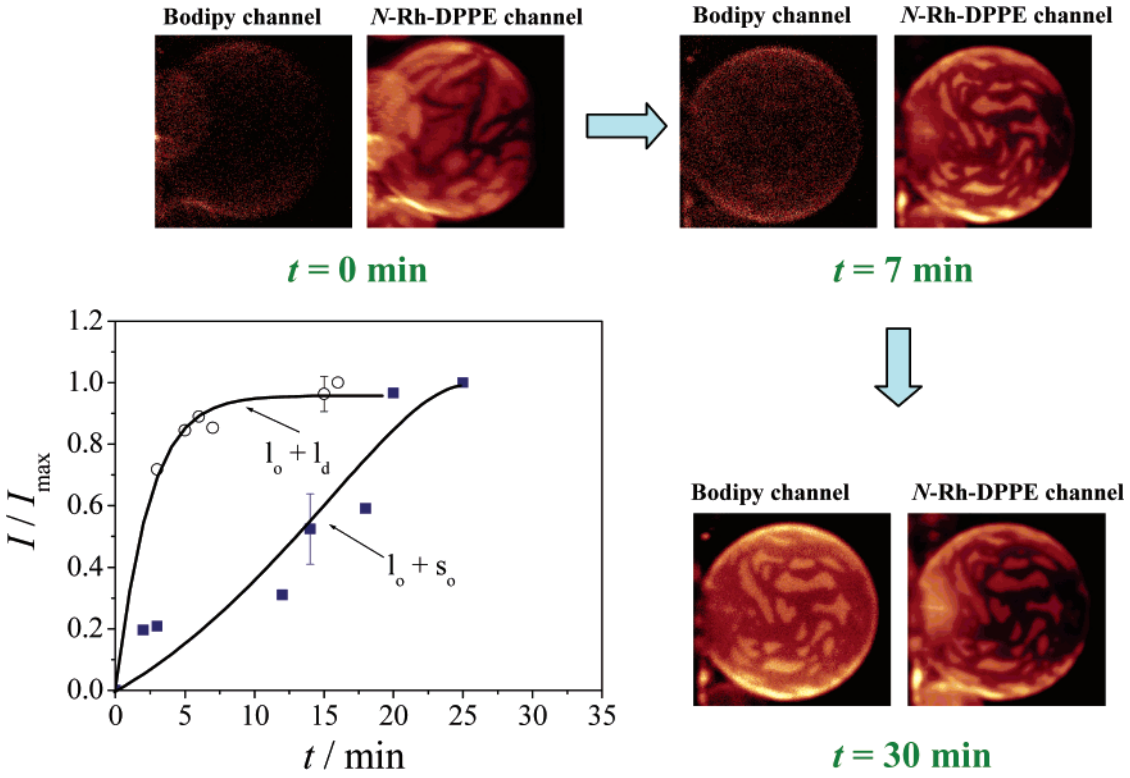

Figure 3. Time-dependent fluorescence intensity images of the system POPC/BSM/cholesterol (25:65:10, $l_o + s_o$ phase region) + *N*-Rh-DPPE with added BODIPY-labeled N-Ras, collected in two channels ($T = 30$ °C). The BODIPY channel monitors the insertion of N-Ras in the GUV (~30 μm); the *N*-Rh-DPPE is a marker for the POPC-rich fluid phase of the system. The first image was taken before the injection of the protein; the other two images were taken 7 and 30 min after the injection of N-Ras to the solution, respectively. The curves shown in the graph represent the kinetic insertion data—in terms of relative changes in BODIPY fluorescence intensity—of N-Ras in different domain-coexisting regions: $l_o + l_d$ (POPC/BSM/Chol 50:25:25) and $l_o + s_o$ (POPC/BSM/Chol 25:65:10), respectively.

the $l_o + s_o$ mixed-domain region (POPC/BSM/cholesterol 25:65:10). Before the insertion at time $t = 0$, the green channel detects few counts, leading to a low fluorescent background only. After about 7 min, it is possible to detect the spherical form of the vesicle in the BODIPY channel as well. The last image was taken after ~30 min, when the binding process of N-Ras to the lipid vesicle is fully completed. The images in both channels coincide, indicating, first, that the protein binds preferentially to the fluidlike domains. However, part of the N-Ras binds, to a much lesser extent, to the s_o domains as well. Second, we notice that the domain shapes do not alter significantly upon incorporation of the dual-lipidated protein.

The rate of the insertion process significantly depends on the type of domains present. The graph also shown in Figure 3 reveals normalized BODIPY fluorescence intensity data taken at 30 °C for lipid systems in the $l_o + l_d$ (POPC/BSM/cholesterol 50:25:25) and in the $l_o + s_o$ (POPC/BSM/cholesterol 25:65:10) phase coexistence regions. The data clearly demonstrate that the binding process is much faster if the lipidated N-Ras partitions into liquid-disordered domains. Embedding N-Ras in the $l_o + s_o$ mixed-domain system is a factor of about 6 slower than that in $l_d + l_o$ mixed-domain vesicles.

Furthermore, we examined and compared the partitioning of N-Ras into the various domains as a function of time (Figure 4). From the equilibrium data, the relative partition coefficient of the lipidated protein in the various phases can be determined by measuring the green channel fluorescence intensity values (I) of the different domains and normalizing them to the mean intensity value of each phase ($\bar{I}_{eq}$). As background, we considered the fluorescence intensity of the channel before the protein was added. Hence, $I/\bar{I}_{eq}$ can be considered a measure of the partition coefficient of the protein between different domains. We found that, in the $l_d + l_o$ mixed-domain system, partitioning of N-Ras into l_d domains is a factor of 1.3 larger than into l_o domains, whereas for the mixture POPC/BSM/cholesterol 25:65:10, representing a $l_o + s_o$ mixed-domain system, binding to l_o domains is favored by a factor of ~2 over solidlike (s_o) domains.

Hence, the phase sequence of preferential binding of N-Ras to mixed-domain lipid vesicles is $l_d > l_o \gg s_o$. The binding kinetics follows a similar order: Binding to l_o domains is about 60% slower than to l_d regions, and binding of N-Ras into s_o domains is ~40% slower than into l_o domains.

AFM Microscopy. AFM measurements on the formation of supported lipid bilayers comprising raft domains have been conducted on different lipid mixtures. After the detection of distinct l_o and l_d domains, the insertion and partitioning of N-Ras in these model biomembranes was studied. Figure 5 shows the AFM images of N-Ras incorporated in a 43:43:14 POPC/BSM/Chol sample, which exhibits l_d and l_o domains (s_o domains, which might also be present in this mixture, cannot be seen, as their contribution is probably too small). Figure 6 shows the corresponding AFM images of N-Ras incorporated in a 2:1:1 POPC/BSM/Chol sample, which, according to the phase diagram presented in Figure 1A should comprise l_d and l_o domains only. The vertical color scale of the images from dark brown to white corresponds to an overall length scale of 20 nm in Figure 5 and 10 nm in Figure 6. Small amounts of the lyophilized lipoprotein was dissolved in 1 mL of H_2O and further diluted 1:10. The samples were removed from the AFM,

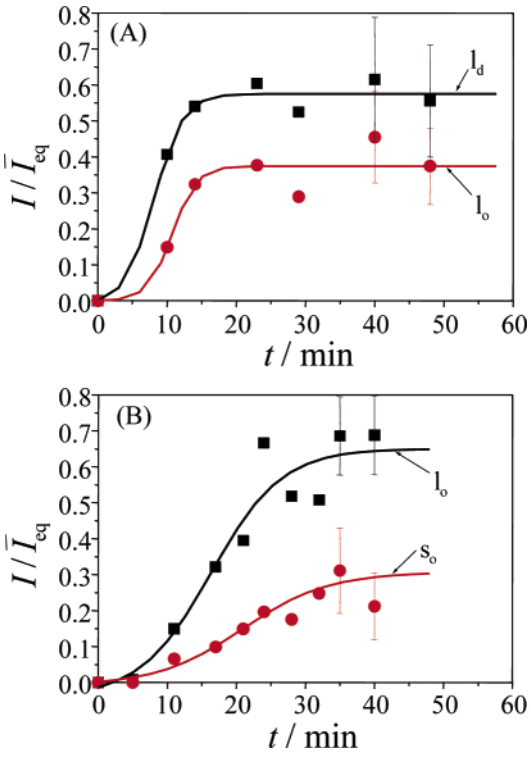

Figure 4. Time-dependent partitioning of hexadecylated and farnesylated N-Ras in the different domains of GUVs composed of (A) POPC/BSM/Chol 50:25:25 ($l_o + l_d$ phase coexistence region) and (B) POPC/BSM/Chol 25:65:10 ($l_o + s_o$ phase coexistence region). As background, the fluorescence intensity of the channel before addition of the protein was taken, and the BODIPY fluorescence intensity values of the different domains were normalized to the mean intensity values of each phase.

and buffer solution was withdrawn and replaced by 20 μL of protein solution and 50 μL of added H_2O. After an incubation time of 30 min, the samples were rinsed with H_2O and replaced in the AFM apparatus. Due to the preparation procedure needed to conduct the AFM measurements, it is not possible to observe the very same region of the lipid bilayer before and after incorporation of N-Ras, and no kinetic measurements could be conducted. Hence, only equilibrium data are presented here. The shape and size of raft domains as well as the loci of incorporated N-Ras appeared to be stable throughout the measurement. In the height image (Figure 5A), raftlike (l_o) protruding domains with sizes from about 50 to 400 nm are clearly visible in light brown above a dark-brown background of l_d phase, and the protein particles appear as white dots. As the lateral resolution is not as high as the vertical one, the existence of some small oligomers cannot be totally ruled out. As has been previously observed, the l_o domains have a thickness about 1 nm larger than that of l_d domains (Figures 5B and 6B).[28] Hence, the location of the protein particles can be efficiently assigned to either l_d or l_o domain areas. The contrast between both lipid domains is enhanced in the phase image of the 43:43:14 POPC/BSM/Chol sample (Figure 5A, right), so that the corresponding areas of the domains can be nicely separated and their relative amounts can be determined. Positions of the protein in either l_d or l_o domains appear differently in the phase image.

By use of image analysis and processing software (ImageJ), the partitioning of the lipidated protein in the various domains was analyzed. Three different regions of protein partitioning were distinguished, with the lateral resolution of the AFM experiment taken into account: l_d bulk, l_d/l_o boundary (width 40 nm), and l_o bulk. The number of protein particles in all regions was counted and normalized to the areas of the corresponding regions. The average ratio of the lipidated protein in bulk l_d domains to protein in l_o domains was found to be 2.9 $\pm$ 1.5; that is, the lipidated protein is clearly preferentially incorporated in the liquid-disordered lipid environment. Interestingly, the overall majority of protein particles associated with raftlike l_o domains is located at the boundaries of the l_o/l_d domains, however (see, e.g., Figure 5A). The average ratio of area-normalized numbers of protein particles located at these raft boundaries to those in bulk raft domains areas was found to be 2.4 $\pm$ 1.0. The analysis of the corresponding AFM images of N-Ras incorporated in the 2:1:1 POPC/BSM/Chol sample, which comprises l_d and l_o domains only, also reveals that the protein is essentially located in l_d domains, and very few (<2%) protein molecules have been observed within bulk l_o domains only. About 50−60% (area-normalized) of the protein molecules were found to be located at the l_o/l_d domain boundaries.

A significant modulation of the fluorescence intensity in the boundary region is not observed, which is probably due to the low spatial resolution of the fluorescence microscopy method. A quantification of minor intensity changes is also difficult, because owing to the low spatial resolution of the fluorescence image, one can also not rule out the existence of smaller domains within the large micrometer domains. In principle, minor differences between the results of the AFM and fluorescence method could also be attributed to the different preparation methods: free-standing GUV of 30 μm diameter containing raft domains of several micrometers size on the one side, and supported bilayers on a mica surface (with mica−bilayer interaction and entropy suppression from reduced membrane undulations) with 10−300 nm sized domains on the other side. In fact, changes in phase transition temperatures and a decoupling of the two opposing leaflets (with the distal monolayer being only slightly affected by the presence of the mica support) have been detected for supported lipid bilayer films recently.[35,54]

Though the lateral resolution of the soft lipid bilayers by AFM is limited to the range of several nanometers, the vertical scale is much better resolved. Figures 5B and 6B show vertical section profiles of the AFM images shown in Figures 5A and 6A, respectively. The protein can be targeted protruding in l_o raft domains as well as in l_d domains, showing the expected height difference of about 3−4 nm, which roughly corresponds to the linear dimension of N-Ras.

Taken together, the AFM results clearly indicate that exogenously added N-Ras spontaneously inserts into canonical raft mixtures and preferentially into liquid-disordered domains, with a large contribution of the lipidated peptide residing in the l_d/l_o boundary region, however. The AFM images locating protein particles at the boundary between both domains thus confirms the proposition from computer simulation work stating that incorporation can be favorable at the domain boundaries as to the possibility to decrease the unfavorable line tension energy.[6,8] A similar patchy localization has been observed for GM1 in DOPC−DPPC monolayers. Insertion of a glycosylphosphatidylinositol- (GPI-) anchored alkaline phosphatase (AP) into raft mixtures showed spontaneous insertion of AP through its GPI anchor into liquid-ordered domains.[33,34]

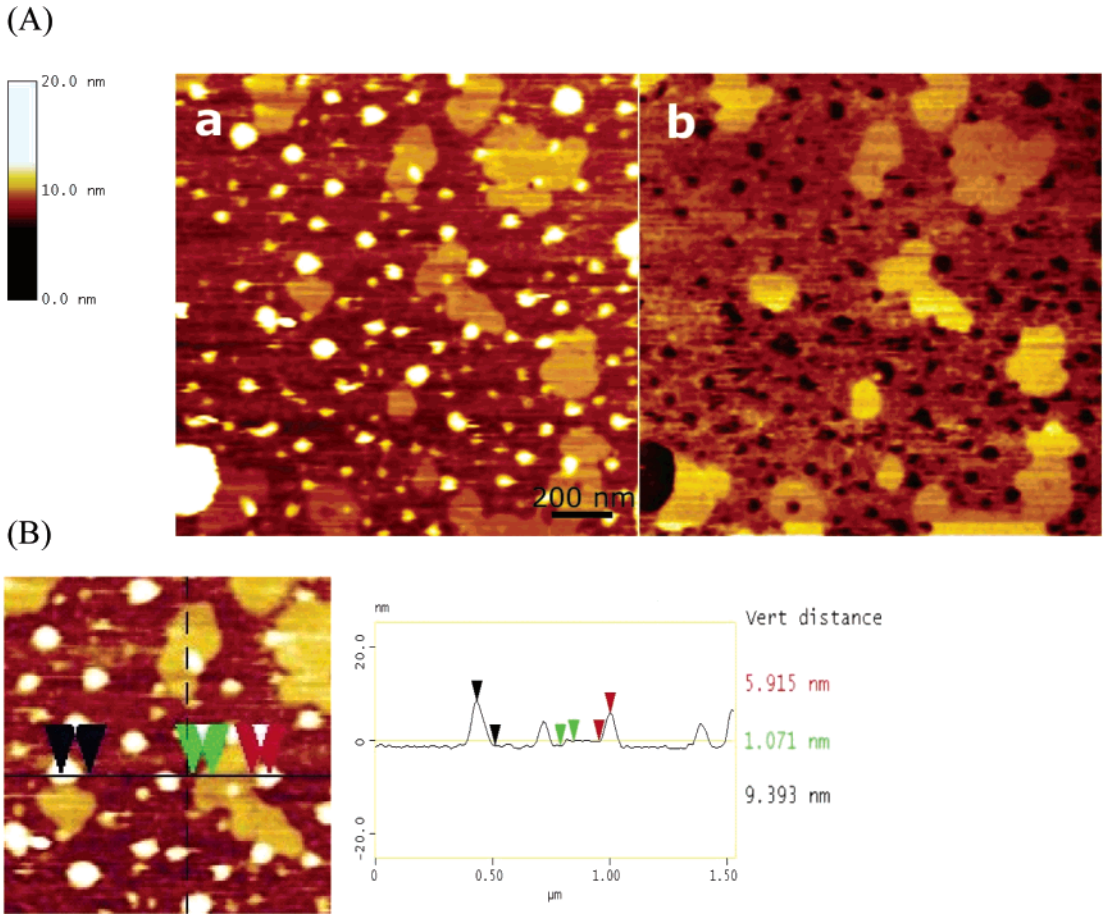

Figure 5. (A) AFM images of N-Ras in POPC/BSM/Chol 43:43:14 (composition c in Figure 1A) supported lipid bilayers ($T = 25$ °C). A few vesicles (e.g., one on the lower left side), which had not fused on the mica surface, appear as big bright spots; (a) height image and (b) phase image. The vertical color scale from dark brown to white corresponds to an overall length of 20 nm. (B) Concomitant section profile of the AFM image. The horizontal black line in the left figure is the localization of the section analysis shown on the right. Vertical distances between pairs of arrows (black, green, red) are given on the right-hand side and are, from left to right, 9.4 nm (black arrows), 1.1 nm (green arrows), and 5.9 nm (red arrows), respectively.

Conclusions

Membrane binding proteins utilizing long, saturated acyl chains, such as GPI-anchored proteins and certain Src family kinases, are able to associate with lipid rafts.[48,49] Myristoylation and palmitoylation of heterotrimeric GTP-binding proteins (G-proteins) was found to be sufficient for association with liposomes and partitioning into rafts.[50] By fluorescence quenching results it has been shown that peptides incorporating isoprenyl groups, by virtue of their branched hydrocarbon chains, or multiply unsaturated phosphatidylcholine, show negligible affinity for l_o domains in mixed-phase $l_o + l_d$ bilayers. Prenylated peptides partition at least 10-fold more weakly into l_o-phase than into l_d-phase lipid vesicles at physiological temperatures.[5,51] By contrast, peptides incorporating multiple S- and/or N-acyl chains, or a cholesterol residue plus an N-terminal palmitoyl chain, show significant partitioning into l_o domains. Lipid-modified peptides with a S-palmitoyl/S-isoprenyl dual-lipidation motif do not seem to promote significant association with l_o domains in ($l_o + l_d$) phase-separated lipid bilayers. Furthermore, it has been shown that the affinity of a lipidated peptide for l_o domains can be strongly influenced not only by the conformation of the lipid substituents but also by the nature and positions of their attachment to the peptide chain.[5,51] In H-Ras, the lipid anchor, comprising a processed CAAX motif and two palmitoyl residues, is assumed to generate affinity to lipid rafts, while the adjacent hypervariable linker region (HVR) provides an attractive force for nonraft plasma membrane domains.[52,53] Upon GTP loading, the interaction between linker domain and elements of nonraft microdomains exceeds the raft preference of the (palmitoyl) lipid anchors, driving the protein to the primary site of H-Ras signaling.[53] Obviously, the GTP/GDP state of H-Ras determines its lateral segregation on the plasma membrane. By contrast, K-Ras is located outside rafts irrespective of bound nucleotide.

The partitioning properties seem to be much less clear in the case of N-Ras, however. Here, only one palmitoyl group is present in the completely processed protein that might be antagonized by the nonraft preference of the isoprenoid group at the C-terminal cysteine.[4] In this spirit, a fraction of partially palmitoylated H-Ras is discussed to prefer cholesterol-indepen-

(49) Melkonian, K. A.; Ostermeyer, A. G.; Chen, J. Z.; Roth, M. G.; Brown, D. A. *J. Biol. Chem.* **1999**, *274*, 3910−3917.
(50) Schroeder, R.; London, E.; Brown, D. *Proc. Natl. Acad. Sci. U.S.A.* **1994**, *91*, 12130−12134.
(51) Moffett, S.; Brown, D. A.; Linder, M. E. *J. Biol. Chem.* **2000**, *275*, 2191−2198.
(52) Wang, T.-Y.; Leventis, R.; Silvius, J. R. *Biophys. J.* **2000**, *79*, 919−933.
(53) Prior, I. A.; Harding, A.; Yan, J.; Sluimer, J.; Pareton, G. R.; Hancock, J. F. *Nat. Cell Biol.* **2001**, *3*, 368−375.
(54) Rotblat, B.; Prior, I. A.; Muncke, C.; Parton, R. G.; Kloog, Y.; Henis, Y. I.; Hancock, J. F. *Mol. Cell. Biol.* 2004, *24*, 6799−6810.
(55) Keller, D.; Larsen, N. B.; Møller, I. M.; Mouritsen, O. G. *Phys. Rev. Lett.* **2005**, *94*, 025701.

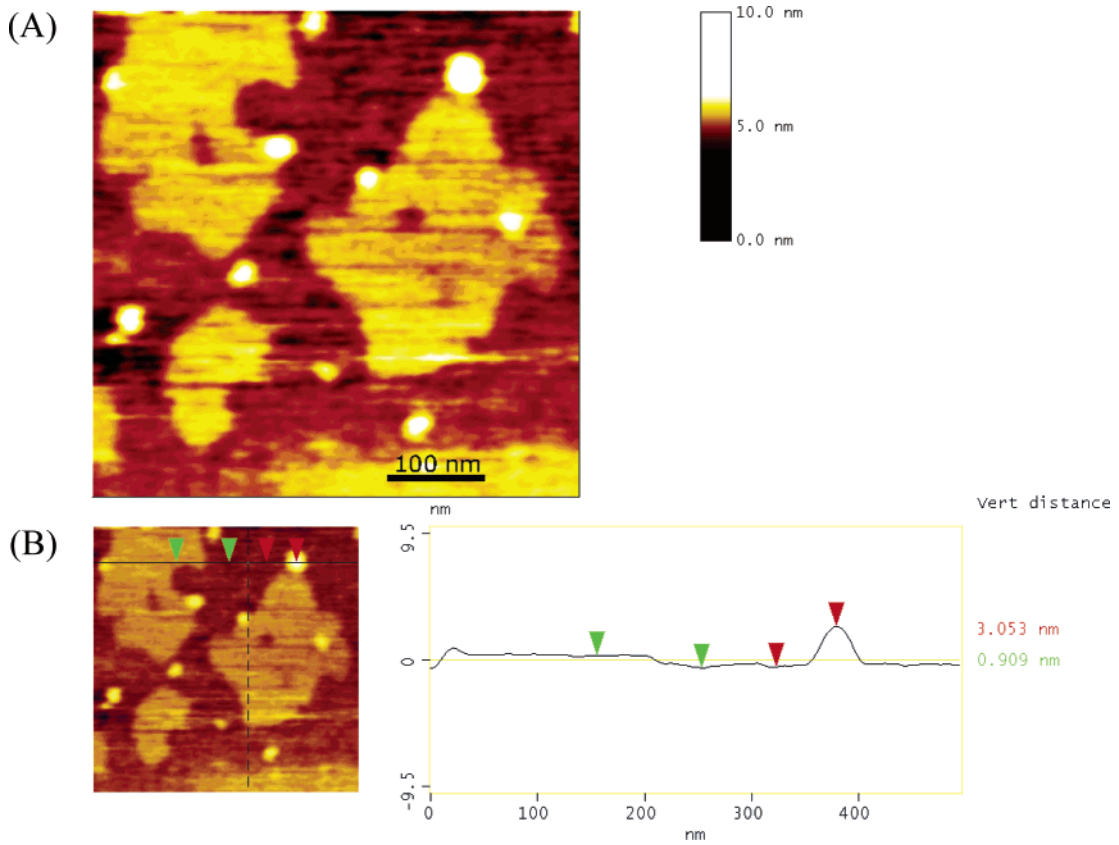

Figure 6. (A) AFM images of N-Ras in POPC/BSM/Chol 2:1:1 (composition a in Figure 1A) supported lipid bilayers ($T = 25$ °C). The vertical color scale from dark brown to white corresponds to an overall length of 10 nm. (B) Concomitant section profile of the AFM image. The horizontal black line in the left figure is the localization of the section analysis shown on the right. Vertical distances between pairs of arrows (green, red) are given on the right-hand side and are 0.909 nm (green arrows) and 3.05 nm (red arrows), respectively.

dent clusters.[36] Hence, after having accomplished the synthesis of the full construct, we decided to investigate insertion of a dual-lipidated N-Ras construct into model raft mixtures of various compositions covering a wide range of length scales by a set of independent techniques.

By combining two-photon excited fluorescence microscopy and tapping-mode AFM, we were able to detect partitioning of a N-Ras lipoprotein in lipid domains of canonical raft mixtures, for the first time, at length scales from the micrometer to the nanometer range. By preparing different lipid mixtures of the system palmitoyloleoylphosphatidylcholine, sphingomyelin, and cholesterol, various coexisting lipid phases ($l_o + l_d$, $l_o + s_o$, and $l_d + l_o + s_o$) could be prepared. Interestingly, whatever the time of incubation, no significant modifications of the surface and shape of the domains were observed during N-Ras insertion in the fluorescence microscopy pictures. The results provide direct evidence that partitioning of hexadecylated and farnesylated N-Ras occurs preferentially in fluidlike liquid-disordered lipid domains, which is also reflected in about 60% faster kinetics of incorporation into the fluid lipid bilayer membrane. To a much lesser extent, the lipidated protein is also embedded in bulk liquid-ordered, raftlike domains. In a $l_o + s_o$ mixed-domain lipid system, binding to l_o domains is taking place as well and is favored by a factor of ~2 over solidlike (s_o) domains. This suggests that the property of the branched farnesyl chain to avoid interactions with cholesterol overrules the preference of long saturated chains, owing to their better packing properties, which leads to stronger van der Waals attraction, for the interaction with Chol and SM in ordered domains. Hence, the phase sequence of preferential binding of N-Ras to mixed-domain lipid vesicles is $l_d > l_o \gg s_o$. Intriguingly, however, as revealed by the better spatial resolution of the AFM data, to a large extent the lipidated protein is located in the boundary region of the domains in mixed-phase liquid-ordered/liquid-disordered bilayers. This might lead to a favorable decrease in line energy (tension), which is associated with the rim of the demixed phases.

Such an interfacial adsorption effect of inserting proteins can generally be expected in many-phase lipid systems that have no particular preferences for any particular phase[6,8]—for example due to hydrophobic mismatch—so that the proteins are expelled to the boundary. It is clear that the localization and accumulation of proteins in the interfaces of a lipid bilayer with domains may provide particularly strong direct protein−protein interactions and hence may serve as a vehicle for protein association. Whereas protein−protein interactions maintain many signaling complexes, specific modifications are believed to be sufficient to sequester proteins in lipid rafts and caveolae. A possible mechanism for effective protein−protein interactions could hence also be a collective association in the interfacial regions of lipid domains.

Acknowledgment. We thank Christine Nowak for excellent technical assistance. Financial support from the Deutsche Forschungsgemeinschaft (SFB 642), the Boehringer Ingelheim Fonds, and the Fonds der Chemischen Industrie is gratefully

acknowledged. The fluorescence microscopy experiments were performed at the Laboratory for Fluorescence Dynamics (LFD) at the University of Illinois at Urbana−Champaign (UIUC). The LFD is supported jointly by the National Center for Research Resources of the National Institutes of Health (PHS 5 P41-RRO3155) and UIUC.

JA055779X